EUROPHYSICS LETTERS

OFFPRINT

Vol. 73 • Number 1 • pp. 35–41

Creation of multi-scale stripe-like patterns in thin polymer blend films

* * *

P. Müller-Buschbaum, E. Bauer, S. Pfister, S. V. Roth, M. Burghammer, C. Riekel, C. David and U. Thiele

Published under the scientific responsibility of the
EUROPEAN PHYSICAL SOCIETY
Incorporating
JOURNAL DE PHYSIQUE LETTRES • LETTERE AL NUOVO CIMENTO

EDP SCIENCES

EUROPHYSICS LETTERS

Europhysics Letter was launched more than fifteen years ago by the European Physical Society, the Société Française de Physique, the Società Italiana di Fisica and the Institute of Physics (UK) and owned now by 17 National Physical Societies/Institutes.

Europhysics Letters aims to publish short papers containing non-trivial new results, ideas, concepts, experimental methods, theoretical treatments, etc. which are of broad interest and importance to one or several sections of the physics community.

Europhysics letters provides a platform for scientists from all over the world to offer their results to an international readership.

EUROPHYSICS LETTERS 1 January 2006

Europhys. Lett., **73** (1), pp. 35–41 (2006)
DOI: 10.1209/epl/i2005-10369-6

Creation of multi-scale stripe-like patterns in thin polymer blend films

P. Müller-Buschbaum[1], E. Bauer[1], S. Pfister[1], S. V. Roth[2], M. Burghammer[2], C. Riekel[2], C. David[3] and U. Thiele[4]

[1] *TU München, Physik-Dept. E13 - James-Franck-Str. 1, 85747 Garching, Germany*
[2] *ESRF - BP 220, F-38043 Grenoble Cedex 09, France*
[3] *Laboratory for Micro- and Nanotechnology, PSI - CH-5232 Villigen, Switzerland*
[4] *MPI für Physik komplexer Systeme - Nöthnitzer Str. 38, D-01187 Dresden, Germany*

received 21 April 2005; accepted in final form 9 November 2005
published online 7 December 2005

PACS. 47.54.+r – Pattern selection; pattern formation.
PACS. 81.05.Lg – Polymers and plastics; rubber; synthetic and natural fibers; organometallic and organic materials.
PACS. 68.15.+e – Liquid thin films.

Abstract. – Multiscale polymeric patterns resulting from flow on an inclined substrate of a binary polymer blend solution of polystyrene and poly-n-butylacrylate in toluene are analyzed with sub-microbeam GISAXS and real space techniques. The locally isotropic phase-separation structure on the 1 micron scale, including a molecular substructure, is embedded in a superstructure on the 100 micron scale of stripe-like variations of film thickness *and* composition oriented perpendicular to the flow direction. It is argued that the multiscale pattern results from the interplay of evaporation, convective flow, differential diffusion and spinodal decomposition.

Driven by applications and basic research the creation of tailor-made polymeric surface structures has been of outmost interest for years. Blending different polymers and thereby conserving their individual properties in the blend is an extremely attractive way to obtain new bulk materials [1] or to coat surfaces by functional films. Such thin polymer blend films provide micron-size surface structures being well adapted to a large variety of applications where the application makes use of mesoscopic length scales in contrast to the nano-structures used in optics [2–5]. In this domain the resulting structures are mainly determined by the used blending ratio and solvent interaction.

Mesoscopic structures produced by drying solutions or suspensions on solid substrates have been extensively studied. For drying drops typical ring patterns were observed [6–8]. These patterns often develop in the close vicinity of the (pinned) three-phase contact line only. As a consequence, the patterned regions are small as compared to the drop size. This allows for interesting applications related to the down-scaling of printed features. Evaporation-assisted patterning was found in a large variety of systems, like solutions of polymers [9], of nano-particles [10] and also of low molecular weight material [11]. The patterning results from a complex interplay of several types of flow with additional distinct mechanisms. For

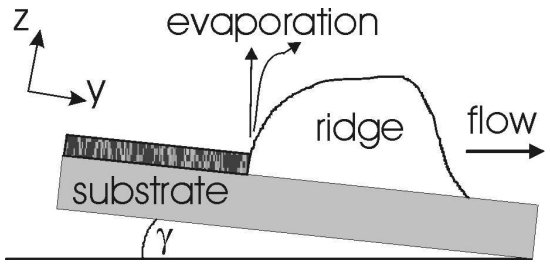

Fig. 1 – Schematic side view of the experimental setting.

instance, the increased evaporation near the contact line drives a convective flow within the drop that transports material towards the periphery [12]. Additionally, an increased solute concentration and a decreased temperature near the contact line may trigger solutal [13] and thermocapillary [14] Marangoni flows. However, also the interaction with the substrate [15] and transversal contact line instabilities [8] have to be taken into account.

Whereas most investigations address nanoparticle-containing suspensions [10, 13], here we focus on a polymer blend solution. Polymer blends are among the most investigated polymeric systems [2]. Beyond their importance for technological applications, they are extremely interesting from a fundamental point of view. Phase separation in polymeric blends takes place on space and time scales more easily accessible experimentally than those of low molecular weight systems. Furthermore, long-range interactions along the chains greatly reduce the size of the critical region, allowing to disregard critical fluctuations in many situations. Thin polymer blend films are prepared on solid supports by various experimental techniques such as solution casting, spin-coating, or dip coating [16]. After solvent evaporation a typical phase-separation structure results [17, 18]. In the thin film regime, phase-separation is accompanied by the creation of marked surface patterns [19]. The morphology (homogeneous film, holes, bi-continuous pattern or drops) as well as the typical lateral size of the surface features depend on key parameters such as blend composition, polymer-polymer interaction parameter and film thickness [20, 21]. This investigation addresses the ability of gravity-driven flow to impose a periodic superstructure onto such patterns (see fig. 1).

Polystyrene (PS) and poly-*n*-butylacrylate (P*n*BA) with molecular weights $M_w = 207\,\mathrm{k}$ ($M_w/M_n = 1.02$) and $M_w = 260\,\mathrm{k}$ ($M_w/M_n = 3.78$), respectively, are blended in a ratio of $3:7\,\mathrm{wt}\%$ in toluene with a concentration of $c = 0.98\,\mathrm{mg/ml}$. The polymer-polymer interaction parameter of PS and P*n*BA is 0.162 at 20 °C [22]. The solution is deposited as a liquid ridge on a slightly inclined ($\gamma = 0.6°$) substrate at room temperature conditions. Prior to deposition the substrate Si(100) with a 1.5 nm native oxide layer was cleaned in an acid bath [23]. Subjected to drying the ridge slides down the incline. In contrast to drying drops the receding three-phase contact line is straight, oriented perpendicular to the base flow, and moves in a quasi-stationary manner. Behind the ridge a thin film of polymeric blend is deposited that turns out to have roughly periodically varying properties along the flow direction.

The variation in blend film thickness is visualized by optical microscopy as shown for a typical sample in fig. 2. The color changes indicate changes in the thickness (see the on-line version). Starting from the left it increases from 170 nm (yellow) to 240 nm (red) and further to 280 nm (blue) as probed with X-ray reflectivity. The next region shows alternating film thicknesses of 240 nm (red) and 280 nm (blue). Centered in fig. 2 is a polymeric bulge that interrupts the region with alternating behavior. It has a mean thickness of several microns. The alternations have a characteristic length scale in flow direction of about 50 microns. Perpendicular to the flow the morphology is homogeneous.

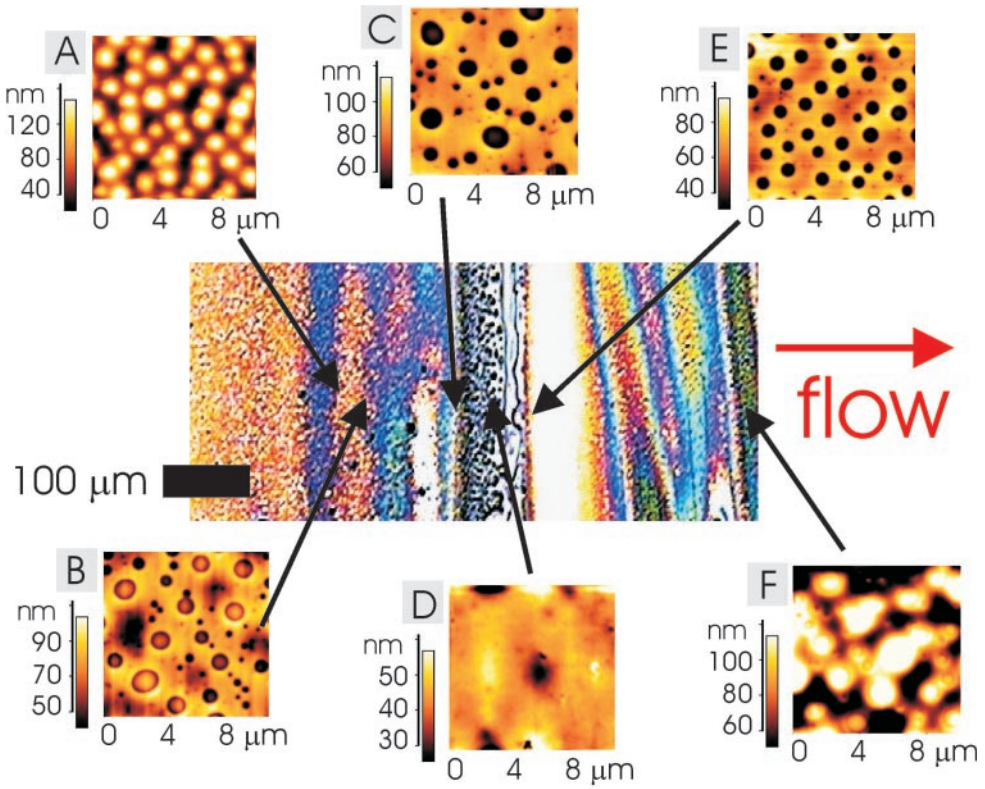

Fig. 2 – The panel shows the real space surface structure as probed with optical microscopy together with selected AFM scans ($10\,\mu$m $\times$ $10\,\mu$m). An Autoprobe CP AFM was operated in tapping mode and the resulting topography data are shown for the positions along the flow direction that are marked by "A" to "F" in fig. 4.

Whereas optical microscopy probes the macroscopic morphology, atomic force microscopy (AFM) detects the local phase-separation structure as shown in fig. 2. Over the scan range of $10\,\mu$m the morphologies are homogeneous, *i.e.* the flow has no local influence. However, the morphology changes significantly between the different positions. Figure 2A shows rather monodisperse drops, fig. 2B drops inside of holes, fig. 2C polydisperse holes, fig. 2D valleys, fig. 2E rather monodisperse holes, and fig. 2F polydisperse drops. Several probed positions perpendicular to the flow show similar morphologies, respectively.

In the usually investigated blend films on horizontal substrates (*i.e.* $\gamma = 0$) [2] one type of morphology is detected and is characteristic for the control parameters such as blend composition, film thickness, polymer-polymer and interface interactions. Flow-induced changes of the latter can be neglected. Changes of the film thickness basically influence the spatial extension of the surface structures whereas the pattern type (*e.g.* drop or hole) remains unchanged [24]. Consequently, we attribute the observed morphology changes to changes in the blend composition. It is known that without flow at the used ratio of PS : P*n*BA = 3 : 7 a pattern of polydisperse drops results [22] similar to fig. 2F. Using the AFM in pulsed force mode shows that the adhesion of the drops is significantly smaller than the one of the surrounding matrix [22]. Because the two polymers differ strongly in the glass transition temperature (T_g(PS) = +104 °C > T_g(P*n*BA) = −34 °C) their mechanical properties at room temperature

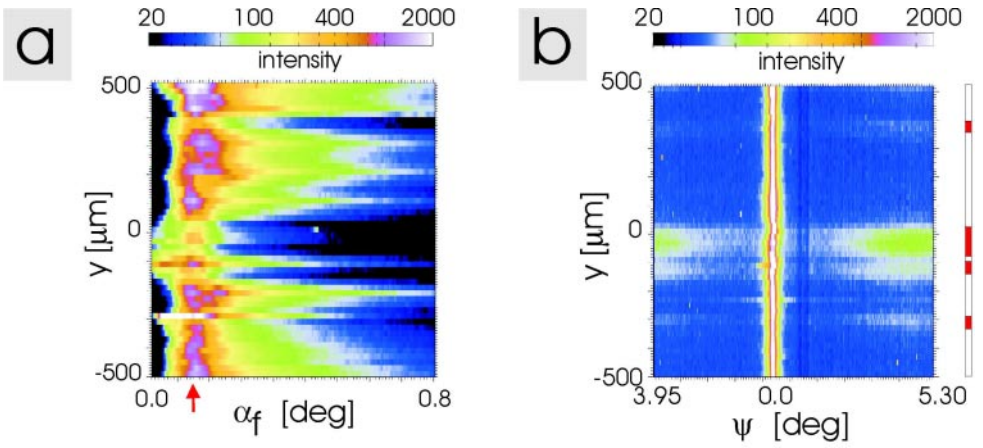

Fig. 3 – With the sub-microbeam GISAXS a region of 1000 μm is scanned in steps of $\Delta y = 20\,\mu$m. a) Close-up of the $(y\alpha_f)$-mapping in the region around the Yoneda peak. Plotted are all vertical cuts from the 2d data as a function of the exit angle α_f at the scanning position y. b) Full $(y\psi)$-mapping: Plotted are all horizontal cuts from the 2d sub-microbeam GISAXS data as a function of the out-of-plane angle ψ at the scanning position y. PS-rich regions are marked by the (red on-line) bars to the right.

differ. PS is glassy and rigid but PnBA is viscous and sticky implying that PS drops sit inside a PnBA matrix. To obtain other morphologies requires a significant change in composition.

We probe the local blend composition and possible internal structures by applying grazing incidence small angle X-ray scattering (GISAXS) [25]. The resolution of the local structure along the flow direction is facilitated by the novel technique of sub-microbeam GISAXS [26]. The experiments use the ID13 beamline (ESRF, Grenoble) at a wavelength of $\lambda = 0.097$ nm (flux of about 10^9 ph/s). The chosen beam diameter of 0.9 μm results in a footprint on the sample of $0.9 \times 52.4\,\mu$m due to the fixed incident angle $\alpha_i = 0.983°$. The long side of the footprint was oriented perpendicular to the flow direction allowing for a set of scans at different positions y along it. Radiation damage was excluded by properly adjusting the exposure to several seconds. Marked features of the 2d sub-microbeam GISAXS scattering pattern ($\alpha_f\psi$-maps) are the Yoneda and the specular peak [25]. The Yoneda peak is located at the position of the critical angle of total external reflection $\alpha_c = \sqrt{2\delta}$, depending on the real part δ of the refractive index, *i.e.* on the material under investigation. For a binary phase separation structure with two different critical angles (PS and PnBA) the Yoneda peak is along the α_f-direction split up in two. The chosen α_i ensures a full probing of the film at each position irrespective of its thickness.

The gradient is scanned for a single typical sample in steps of $\Delta y = 20\,\mu$m. The characteristic features of 50 GISAXS patterns are extracted by composing respective vertical cuts at the central region ($\psi = 0$) for different positions y into one $(y\alpha_f)$-map. This is shown in fig. 3a for a range of α_f that emphasizes the intensity distribution of the split Yoneda peak (marked by the arrow). Taking the transmission functions into account, its varying intensity allows to calculate the relative amount of PnBA in the blend [25].

The found variations in blend composition are plotted in fig. 4. They confirm our earlier hypothesis that the flow induces variations of the film thickness *and* the composition of the polymeric blend. As a consequence, it is responsible for the different morphologies displayed in fig. 2. This overall picture is further confirmed as at the initial concentration of PS : PnBA =

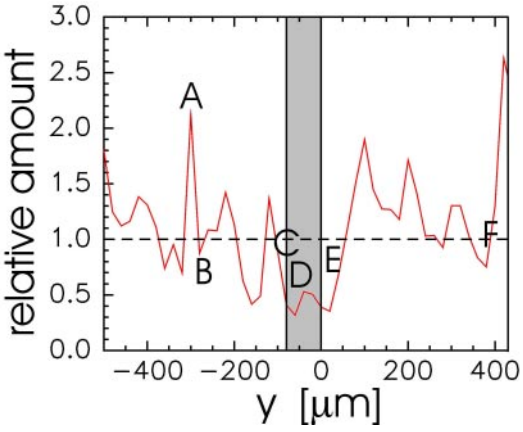

Fig. 4 – Relative amount of P*n*BA as a function of the position y along the flow direction as determined by the scattering experiment (solid line). The dashed line and the gray shaded area mark the nominal P*n*BA concentration and the region of the polymeric bulge, respectively. Letters "A"-"F" mark positions probed by AFM.

3 : 7 structures are found (fig. 2F) equal to those observed without flow [2]. An increase of the P*n*BA content reduces the size of the PS domains and smaller drops are observed (fig. 2A). A slight decrease of the P*n*BA content results in the coexistence of drops and holes (fig. 2B), whereas a strong decrease results in a change of the morphology towards a PS matrix with P*n*BA filled holes (figs. 2C and E). A further decrease reduces number and depth of the holes (fig. 2D). The reversal of the components forming the matrix and the dispersed phase agrees well with observations of binary films without flow but for a significant change in the blend composition [2].

What is the mechanism leading to the formation of stripe-like thickness and composition patterns on the 100 micron scale? One can exclude a direct effect of the flow-induced shear on the decomposition of the polymeric blend [27,28] because it would lead to anisotropic patterns on the scale of fig. 2. The mesoscopic length scale and the orientation parallel to the receding contact line indicates that the pattern is due to a longitudinal instability of the movement of the contact line as the one observed in the physisorption during dynamic Langmuir wetting [29]. We propose on a qualitative level a mechanism based on a coupling between the velocity of the receding contact line, the differential transport of the two dissolved polymers in the solvent and the composition of the deposited layer. It is based on the assumption that all relevant transport occurs close to the contact line, *i.e.* in the diffuse boundary layer of the flow. This implies that even a small contrast in the diffusion coefficients of the polymers is highly relevant.

The concentrations of the polymers in the wedge at the receding contact line are determined by the convective flow and the differential diffusion in the wedge, and the deposition of the blend film behind the wedge. The convective flow is a superposition of a gravitationally driven downward flow and an evaporation-induced Marangoni upward flow. These lead together with the enhanced evaporation at the contact line to a proportional increase of the concentration of both polymers in the wedge. However, the equilibrating diffusion is not equally strong for the two polymers. According to the mass differences in toluene PS diffuses faster away from the wedge than P*n*BA resulting in an increase of the P*n*BA concentration in the deposited polymer blend. The exact increase depends on the ratio of convective, diffusive and evaporative

time scales. Using the Young-Laplace equation and assuming that the interface tensions of the solution with air and the substrate are approximately constant one finds that the increase leads to a smaller equilibrium contact angle because $\gamma_{PnBA} \approx 34\,\mathrm{mN/m} < \gamma_{PS} \approx 41\,\mathrm{mN/m}$ [22]. This decreases the difference between dynamic and equilibrium contact angles, *i.e.* the velocity of the receding contact line. This in turn favors the differential diffusion as compared to convection and evaporation thereby leading to a positive feedback, *i.e.* an instability. However, nonlinearly the instability will saturate due to the deposition-forced depletion of the P*n*BA. The interplay of instability and saturation leads then to a stripe-like deposition pattern.

Note that the polydisperse P*n*BA consists of chains of various lengths. However, short chains are located preferentially at interfaces, thus the mean diffusion of P*n*BA within the wedge will be even slower than for a 260 k chain. In addition, we emphasize that in a linear instability unstable modes grow exponentially even if the differences in the mean diffusivities or the equilibrium contact angles are arbitrary small. The magnitude of the difference only determines the growth rate of the instability and in consequence has an influence on the length scale of the observed stripe pattern.

The proposed mechanism is supported by the experimental observation of a smaller period of the stripe-like pattern for a slight increase of the inclination. Such an increase leads to a larger sliding velocity and a smaller receding dynamic contact angle [30]. The accompanying increase of the importance of the convection as compared to evaporation and diffusion does not interfere with the instability mechanism itself but diminishes the absolute effect of the differential diffusion. Therefore lower P*n*BA concentrations are reached, saturation is faster and the period of the stripes becomes smaller. A further slight increase of the inclination triggers transversal instabilities of the receding contact line [31] and leads to more complex patterns.

While AFM scans characterize only morphology and mechanical properties, GISAXS also detects buried structures down to the molecular size. Most prominent in-plane lengths are detected from the analysis of the ψ-dependence of the GISAXS data [26]. As before we use the 50 scattering patterns but now choose horizontal cuts at the critical angle of PS to compose a single $(y\psi)$-map (fig. 3b). The region at $\psi = 0$ is dominated by the resolution of the set-up. A high intensity is characteristic for large lateral lengths such as displayed in the AFM and optical data. Here we focus on smaller length scales comparable to the size of the polymer molecules. The broad peaks visible in fig. 3b at large ψ values indicate a most prominent internal lateral length of 1.5 nm. This adds a third length scale to our picture. The substructure is present in the polymeric bulge and in other regions with strongly increased PS content (marked by red on-line bars at the right of fig. 3b). Regions with larger P*n*BA content do not exhibit any substructure. As a consequence, it is very likely that the smallest observed structure results from the different mechanical properties of the majority component. Cavities, introduced by the competition of flow and drying, relax in case of a remaining mobility of the matrix and no nano-structure is observed in P*n*BA rich regions. In contrast, at room temperature the PS matrix remains rigid and may form crazes under mechanical stress as reported in ref. [32]. Typically, these crazes have about the observed size, depending on the stress induced [33].

In summary, we have demonstrated that the receding contact line of an evaporating solution of a specific polymeric blend flowing on an incline produces complex multi-scale patterns. A costly GISAXS study has allowed to establish stripe-like variations of *both*, surface height and composition of the deposited polymer layer. The proposed instability mechanism responsible for the patterning is based on i) faster bulk mean diffusion of PS than of P*n*BA and ii) larger solvent equilibrium contact angle on PS than on P*n*BA. This leads us to the hypothesis that a continuously receding contact line can be used as a general tool to produce parallel thickness *and* composition patterns on the 100 micron scale accompanied by different locally homogeneous 1 micron scale morphologies. A future detailed theory will have to be based on

an extended model-H [34] incorporating free surface, evaporation, and driven contact line. We hope that our experimental result and heuristic explanation triggers further work that tests our hypothesis.

* * *

We thank M. Stenert and F. Bandermann for supplying the P*n*BA and the DFG SPP 1164 "Nano- and Microfluidics" (Mu1487/2) for financial support. UT acknowledges support through the EU MRTN-CT-2004–005728.

REFERENCES

[1] Ryan A. J., *Nature Mater.*, **1** (2002) 8.
[2] Geoghegan M. and Krausch G., *Prog. Polym. Sci.*, **28** (2003) 261.
[3] Walheim S. *et al.*, *Science*, **283** (1999) 520.
[4] Russell T. P., *Science*, **297** (2002) 964.
[5] Fasolka M. J. and Mayes, A. M., *Annu. Rev. Mater. Res.*, **31** (2001) 323.
[6] Adachi E. *et al.*, *Langmuir*, **11** (1995) 1057.
[7] Deegan R. D. *et al.*, *Nature*, **389** (1997) 827.
[8] Deegan R. D., *Phys. Rev. E*, **61** (2000) 475.
[9] Kimura M. *et al.*, *Langmuir*, **19** (2003) 9910.
[10] Moriarty P. *et al.*, *Phys. Rev. Lett.*, **89** (2002) 248303.
[11] Cavallini M. and Biscarini F., *Nano Lett.*, **3** (2003) 1269.
[12] Gonuguntla M. and Sharma A., *Langmuir*, **20** (2004) 3456.
[13] Nguyen V. X. and Stebe K. J., *Phys. Rev. Lett.*, **88** (2002) 164501-1.
[14] Haw M. D. *et al.*, *Langmuir*, **18** (2002) 1626.
[15] Warner M. R. E. *et al.*, *Colloid Interface Sci.*, **267** (2003) 92.
[16] Krausch G., *Mater Sci. Eng. R*, **14** (1995) issues 1-2, pp. v-vi.
[17] Jones R. A. L. *et al.*, *Phys. Rev Lett.*, **62** (1989) 280.
[18] Bruder F. and Brenn R., *Phys. Rev Lett.*, **69** (1992) 624.
[19] Wang H. and Composto R. J., *Europhys. Lett.*, **50** (2000) 1659.
[20] Gutmann J. S. *et al.*, *Faraday Discuss.*, **112** (1999) 285.
[21] Müller-Buschbaum P. *et al.*, *Macromolecules*, **33** (2000) 4886.
[22] Stenert M., PhD Thesis, University Essen (2000); Stenert M. *et al.*, *e-Polymers*, **15** (2004) 1.
[23] Müller-Buschbaum P., *Eur. Phys. J. E*, **12** (2003) 443.
[24] Müller-Buschbaum P. and Stamm M., *Colloid Polym. Sci.*, **279** (2001) 376.
[25] Salditt T. *et al.*, *Europhys. Lett.*, **32** (1995) 331.
[26] Müller-Buschbaum P. *et al.*, *Physica B*, **357** (2005) 148.
[27] Chan C. K. *et al.*, *Phys. Rev. Lett.*, **61** (1988) 412.
[28] Hashimoto T. *et al.*, *Phys. Rev. Lett.*, **74** (1995) 126.
[29] Spratte K. *et al.*, *Europhys. Lett.*, **25** (1994) 211.
[30] Dussan E. B., *Annu. Rev. Fluid Mech.*, **11** (1979) 371.
[31] Studied for simple liquids in Thiele U. and Knobloch E., *Phys. Fluids*, **15** (2003) 892.
[32] Brown H. R. and Kramer E. J., *J. Macromol. Sci.-Phys. B*, **19** (1981) 487.
[33] Lorenz-Haas C. *et al.*, *Langmuir*, **19** (2003) 3056.
[34] Hohenberg P. C. and Halperin B. I., *Rev. Mod. Phys.*, **49** (1977) 435.